A reduced complexity model of a gravel-sand river bifurcation
Equilibrium states and their stability

Schielen, Ralph M.J.; Blom, Astrid

DOI
10.1016/j.advwatres.2018.07.010

Publication date
2018

Document Version
Accepted author manuscript

Published in
Advances in Water Resources

Citation (APA)
Schielen, R. M. J., & Blom, A. (2018). A reduced complexity model of a gravel-sand river bifurcation: Equilibrium states and their stability. *Advances in Water Resources*, *121*, 9-21. https://doi.org/10.1016/j.advwatres.2018.07.010

Important note
To cite this publication, please use the final published version (if applicable).
Please check the document version above.

A reduced complexity model of a gravel-sand river bifurcation: Equilibrium states and their stability

Ralph M.J. Schielen

Faculty of Engineering Technology, University of Twente, Netherlands
Ministry of Infrastructure and Water Management - Rijkswaterstaat, Netherlands

Astrid Blom

Faculty of Civil Engineering and Geosciences, Delft University of Technology, Netherlands

Abstract

We derive an idealized model of a gravel-sand river bifurcation and analyze its stability properties. The model requires nodal point relations that describe the ratio of the supply of gravel and sand to the two downstream branches. The model predicts changes in bed elevation and bed surface gravel content in the two bifurcates under conditions of a constant water discharge, sediment supply, base level, and channel width and under the assumption of a branch-averaged approach of the bifurcates. The stability analysis reveals more complex behavior than for unisize sediment: three to five equilibrium solutions exist rather than three. In addition, we find that under specific parameter settings the initial conditions in the bifurcates determine to which of the equilibrium states the system evolves. Our approach has limited predictive value for real bifurcations due to neglecting several effects (e.g., transverse bed slope, alternate bars, upstream flow asymmetry, and bend sorting), yet it provides a first step in addressing mixed-size sediment mechanisms in modelling the dynamics of river bifurcations.

Keywords: river bifurcation, mixed-size sediment, idealized model, equilibrium, stability analysis

1. Introduction

River bifurcations or diffluences are found in alluvial fans, braided rivers, anabranching rivers, deltas, cut-off channels, diversions (for flood control or water intakes), and in constructed side channels that are part of river restoration schemes. Once a bifurcation is initiated, a downstream channel (or bifurcate or distributary) continues to deepen as long as the sediment transport capacity exceeds the sediment supply to the channel.

Sediment transport in a channel consists of bed-material load (i.e., bed load and suspended bed-material load) and wash load (*Paola*, 2001; *Church*, 2006).

As wash load is typically assumed to be distributed uniformly over the water column, it is assumed to be partitioned over the bifurcates according to the ratio of the water discharge.Bed-material load, however, partitions over the bifurcates in a less straightforward manner. The partitioning of sediment in streams dominated by suspended bed-material load depends on the initial flow depth and channel slope in the bifurcates (*Slingerland and Smith*, 1998), the grain size of the bed sediment (*Slingerland and Smith*, 1998), and curvature-induced effects in the upstream channel (*Hackney et al.*, 2017). The partitioning of sediment in bed load dominated streams depends on:

- the conditions in the bifurcates: base level, channel width, friction, bifurcation angle (*Bulle*, 1926; *Tarekul Islam et al.*, 2006; *Van der Mark and Mosselman*, 2013), and the zones of flow recirculation close to the bifurcation (*Bulle*, 1926; *De Heer and Mosselman*, 2004; *Thomas et al.*, 2011; *Marra et al.*, 2014), vegetation (*Burge*, 2006), and cohesive sediment and bank erosion (*Miori et al.*, 2006; *Zolezzi et al.*, 2006);

- the conditions in the area just upstream of the bifurcation: the transverse distribution of water and sediment over the upstream channel, which is affected by secondary flow (*Van der Mark and Mosselman*, 2013), a transverse bed slope induced by an inlet step (*Bolla Pittaluga et al.*, 2003), alternate bars (*Bertoldi and Tubino*, 2007; *Bertoldi et al.*, 2009; *Redolfi et al.*, 2016), and sediment mobility (*Frings and Kleinhans*, 2008);

- conditions extending further upstream: flow asymmetry induced by a bend, which tends to provide one bifurcate with a larger fraction content of the flow and the other one with a larger fraction content of the sediment load (*Federici and Paola*, 2003; *Kleinhans et al.*, 2008; *Hardy et al.*, 2011; *Van Dijk et al.*, 2014) and transverse sediment sorting due to bend flow (*Sloff et al.*, 2003; *Frings and Kleinhans*, 2008; *Sloff and Mosselman*, 2012).

The partitioning of the sediment load over the bifurcates determines whether the bifurcation develops towards a stable state with two open downstream branches or a state in which the water discharge in one of the branches continues to increase at the expense of the other branch. The latter case may lead to the silting up of one of the downstream channels. Under such conditions a one channel configuration is a stable equilibrium solution of the bifurcation system (*Wang et al.*, 1995), yet in literature this situation is often termed an 'unstable bifurcation' (*Federici and Paola*, 2003; *Burge*, 2006), as the two channel system ceases to exist.

Early one-dimensional reduced complexity models describing the development towards the equilibrium states of two bifurcates have been developed for bed load transport in sand-bed rivers (*Wang et al.*, 1995), bed load transport in gravel-bed rivers (*Bolla Pittaluga et al.*, 2003), and suspended bed-material load (*Slingerland and Smith*, 1998). Such reduced complexity models allow for the computation of the partitioning of the water discharge as the water surface

elevation at the bifurcation point must be equal between the three reaches. The sediment partitioning, however, depends on the geometry of the bifurcation and the three-dimensional flow structure, which obviously cannot be reproduced by a one-dimensional model. A one-dimensional model therefore requires a nodal point relation that describes the partitioning of the sediment load over the bifurcates.

Wang et al. (1995) were the first to introduce a nodal point relation describing the partitioning of the sediment supplied from upstream over the bifurcates. They then apply a simpler form of their nodal point relation ($\bar{s}_1/\bar{s}_2 = (q_1/q_2)^k$, where $\bar{s}_{1,2}$ is the rate of sediment supply per unit width to branches 1 and 2 and $q_{1,2}$ is the water supply per unit width to branches 1 and 2) to analyse the stability of the solutions to the equilibrium morphodynamic state of the bifurcates. Studying avulsion development (*Slingerland and Smith*, 1998) introduce a nodal point relation that originates from integration of the vertical concentration profile of the suspended sediment. Alternative nodal point relations have been developed by *Bolla Pittaluga et al.* (2003), who account for the effects of a transverse bed slope that induces lateral sediment transport to the deeper bifurcate, and *Kleinhans et al.* (2008), who account for the effects of an upstream bend, both of which will be addressed in further detail below.

Pioneering work on bifurcation dynamics using a nodal point relation was conducted by *Wang et al.* (1995): they assume a constant water discharge and sediment supply rate in the upstream channel, a constant and equal base level in the two bifurcating branches, and unisize sediment conditions. They apply the *Engelund and Hansen* (1967) sediment transport relation without a threshold for significant transport: $s \propto U^n$, where s denotes the sediment transport capacity per unit width, U the depth-averaged flow velocity, and n is the exponent in the power law load relation ($n = 5$). They find that for $k < n/3$ the equilibrium solution where one of the bifurcates closes is stable, whereas for $k > n/3$ the equilibrium solution with two open branches is stable. Despite these early results a model for k is still lacking. Also *Slingerland and Smith* (1998) reveal that a bifurcation or avulsion develops towards a stable state with two open downstream branches or a state in which one channel becomes the dominant channel at the expense of the other branch.

In such strongly idealized one-dimensional analyses, two-dimensional and three-dimensional effects near the bifurcation point are not readily accounted for. One of these effects is the Bulle effect (*Bulle*, 1926; *Van der Mark and Mosselman*, 2013; *Dutta et al.*, 2017), which indicates a situation where the sediment supply to a diversion channel (i.e., a channel that branches off the main channel under a certain angle) is significantly larger than the diversion channel's fraction content of the water discharge. This effect is associated with secondary flow *Thomas et al.* (e.g., 2011). Another effect is the difference in bed elevation that is associated with a difference in flow depth between the two bifurcates (e.g., *Bolla Pittaluga et al.*, 2003; *Kleinhans et al.*, 2013). This bed elevation difference (also denoted using the term inlet step) tends to increase the sediment supply to the deeper bifurcate (e.g., *Slingerland and Smith*, 1998), which acts as a stabilizing mechanism.

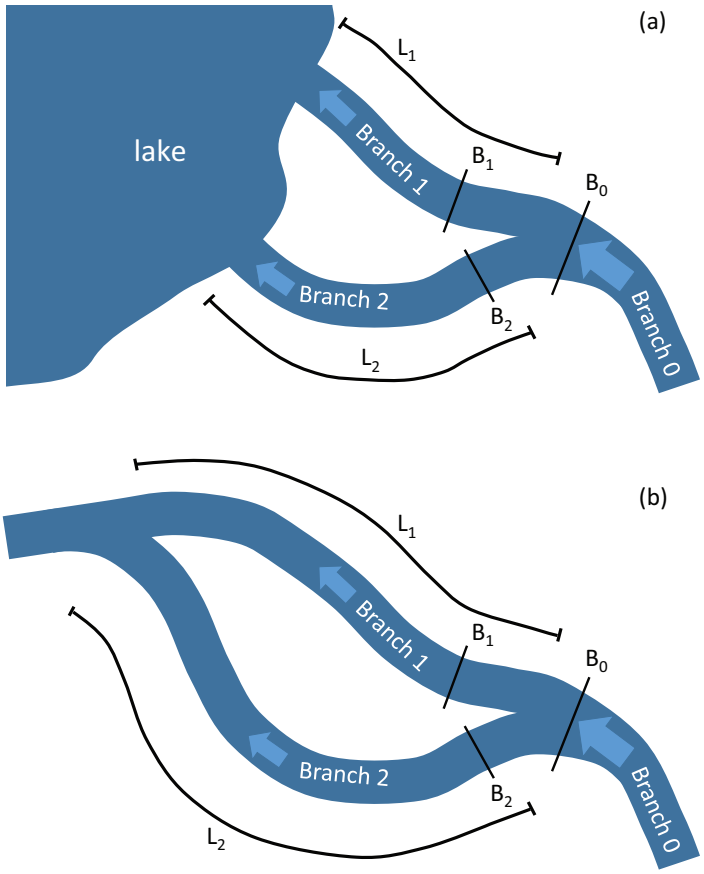

Figure 1: Schematic of (a) a channel (branch 0) bifurcating into two channels (branches 1 and 2) flowing into a lake characterized by the same base level (*Wang et al.*, 1995) and (b) a side channel system. Our analysis and model are applicable to both cases.

Although mixed-size sediment systems may reveal behavior that is essentially different from unisize sediment systems (*Sinha and Parker*, 1996; *Mosselman and Sloff*, 2008; *Blom et al.*, 2016, 2017a,b), so far the influence of noncohesive mixed-size sediment on bifurcation dynamics has not been studied explicitly. Wash load, suspended bed-material load, and bed load (*Paola*, 2001; *Church*, 2006) are expected to respond differently to the above-mentioned mechanisms (*Hackney et al.*, 2017). Mixed-size sediment effects are the following:

1. As the vertical profile of sediment concentration is less uniform over depth for coarse sediment (i.e., coarse sediment tends to concentrate more strongly near the bed), coarse sediment tends to be affected more by an inlet step than fine sediment (*Slingerland and Smith*, 1998).
2. The effect of the transverse bed slope on lateral transport upstream of the bifurcation depends on grain size, where coarse sediment is affected by the transverse bed slope more strongly than fines (*Parker and Andrews*, 1985);
3. The presence of a bend upstream of the bifurcation typically leads to bend sorting and a coarser sediment supply to the distributary in the outer bend than to the one in the inner bend (*Sloff et al.*, 2003; *Frings and Kleinhans*, 2008; *Sloff and Mosselman*, 2012);
4. Alternate bar formation and geometry appear to be affected by the grain size distribution of the sediment mixture (*Lanzoni*, 2000; *Bertoldi and Tubino*, 2005).

Our objective is to assess the elementary consequences of the introduction of mixed-size sediment mechanisms in the modelling of the dynamics of a river bifurcation. To this end we follow *Wang et al.* (1995)'s approach and its simple nodal point relation with associated limitations and simplifications: we neglect the effects of vegetation, cohesive sediment, bank erosion, alternate bars or a bend in the upstream channel, as well as the Bulle effect and the transverse slope effect. We extend their model to conditions with bed-material load of a two-fraction sediment mixture consisting of gravel and sand. This implies the need for two nodal point relations describing the ratio of, respectively, the gravel and sand supply to the two bifurcates. We study the stability of the equilibrium states of the bifurcates in an engineered river characterized by a fixed channel width.

The proposed analysis and model are applicable to both cases shown in Figure 1: a bifurcation system with two bifurcates that are characterized by the same base level and a side channel system. We set up a model describing the equilibrium solutions of the mixed sediment bifurcation system (section 2), we determine its equilibrium solutions (section 3), we derive a system of ordinary differential equations for the flow depth and bed surface texture in the bifurcates (section 4), and perform a stability analysis of the equilibrium solutions (section 5). The analysis also provides insight on the time scale of the evolution towards the stable equilibrium solutions (section 6).

2. Model of the equilibrium state

In this section we strongly simplify the situation of a gravel-sand river bifurcation, describe the problem from a mathematical point of view, and list the governing equations. To this end we consider an engineered river with a fixed channel width that may vary between the branches, a temporally constant water discharge in the upstream branch (i.e., branch 0 in Figure 1) and a temporally constant gravel supply rate and constant sand supply rate to the upstream branch.

Under equilibrium conditions ($\partial/\partial t = 0$) without subsidence, uplift, and particle abrasion, the equation describing conservation of sediment mass (i.e. the Exner equation) reduces to the the stationary Exner equation, $\partial S_i/\partial x = 0$, where S_i denotes the sediment transport capacity in branch i, the subscript i indicates branch i, and x is the streamwise coordinate. In other words, by definition the sediment transport capacity S_i equals the sediment supply to branch i, $\bar{S}_i$, where the bar indicates the sediment supply.

For simplicity we apply the Engelund and Hansen power law load relation (*Engelund and Hansen*, 1967):

$$S_i = B_i m_i U_i^n \tag{1}$$

in which $m_i = G_i/D$ with D denoting a characteristic grain size, $G_i = 0.05/(C_i^3 R^2 g^{1/2})$, U_i the depth-averaged flow velocity, B_i the channel width, C_i the Chézy friction coefficient, g denotes the gravitational acceleration, and R the submerged density ($R = (\rho_s - \rho)/\rho$ where ρ_s and ρ are the mass density of, respectively, sediment and water). For simplicity we assume that m_i does not vary between the branches ($m_i = m$), which implies that also the friction coefficient and the coefficient G do not vary between the branches ($C_i = C$, $G_i = G$).

Combination of equation (1) with the stationary Exner equation illustrates that under equilibrium conditions where the channel width and friction do not vary spatially, besides the sediment transport rate, also the flow velocity is uniform.

The flow is described using the one-dimensional conservation equations for water mass and streamwise momentum, i.e. the Saint-Venant equations (*Saint-Venant*, 1871). Under equilibrium conditions, the conservation equation for water mass is simplified to $\partial Q_i/\partial x = 0$ (where Q_i denotes the water discharge in branch i, see Figure 1), which implies

$$Q_i = B_i U_i H_i = const \tag{2}$$

where H_i denotes the flow depth (Figure 2). As the flow velocity is uniform over the branch, equation (2) implies that also the flow depth does not vary over the branch.

Under equilibrium conditions the conservation equation for streamwise momentum of the flow reduces to the backwater equation. For a uniform flow

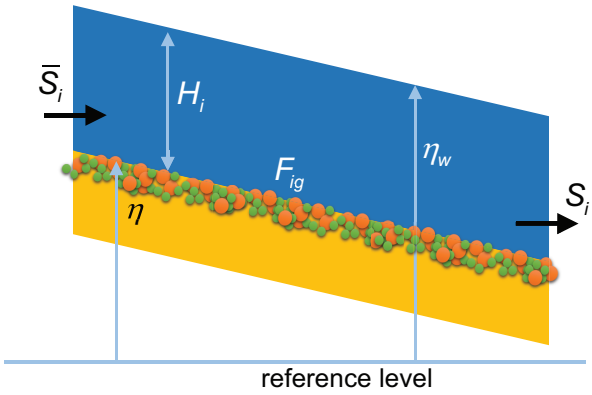

Figure 2: Definition of symbols.

depth, the backwater equation reduces to the normal flow equation:

$$H_i = \left(\frac{Q_i^2}{i_i C^2 B_i^2} \right)^{1/3} \tag{3}$$

where i_i denotes the channel slope. For simplicity, the Chézy friction coefficient C is assumed independent of the bed surface texture and flow conditions and hence constant.

Under mixed-size sediment conditions, the Exner equation is replaced by the equations for the conservation of gravel and sand mass at the bed surface, i.e. the Hirano equations (*Hirano*, 1971; *Ribberink*, 1987; *Parker*, 1991). Under equilibrium conditions the Hirano equations reduce to $\partial S_{ig}/\partial x = \partial S_{is}/\partial x = 0$, where the subscripts g and s indicate gravel and sand, respectively, and S_{ig} and S_{is} denote, respectively, the gravel and sand transport capacities in branch i. This implies that in an equilibrium state without particle abrasion the gravel and sand load do not vary within a branch (e.g., *Blom et al.*, 2016). For simplicity we apply the Engelund and Hansen power law load relation in a fractional manner (*Blom et al.*, 2016, 2017a) and replace equation (1) by

$$S_i = S_{ig} + S_{is} \tag{4}$$

$$S_{ig} = F_{ig} B_i m_g U_i^n \tag{5}$$

$$S_{is} = (1 - F_{ig}) B_i m_s U_i^n \tag{6}$$

where F_{ig} denotes the volumetric fraction content of gravel at the bed surface in branch i or, briefly, the surface gravel content (Figure 2), and $m_g = G/D_g$ and $m_s = G/D_s$ with D_g and D_s the grain sizes of, respectively, gravel and sand. Obviously the coefficients m_g and m_s have different values. Similarly to the unisize case, we assume m_g not to vary between the branches. The same holds for m_s. Combination of equations (5) and (6) with the stationary Hirano and Saint-Venant equations shows, analogous to the unisize sediment case, that

(under equilibrium conditions without uplift, subsidence, and particle abrasion) the flow velocity, flow depth, and surface gravel content do not vary within a branch.

The model requires a nodal point relation that relates the ratio of the sediment supply to the downstream branches to the ratio of the water discharge. The nodal point relation introduced by *Wang et al.* (1995) is applicable to unisize sediment conditions:

$$\bar{s}^* = \alpha q^{*k}, \quad \text{or} \quad \frac{\bar{s}_1}{\bar{s}_2} = \alpha \left(\frac{q_1}{q_2}\right)^k \tag{7}$$

where $\bar{s}_i$ denotes the rate of sediment supply per unit width to branch i, the superscript $*$ indicates the ratio of the values of the specific variable for branches 1 and 2 (e.g., $\bar{s}^* = \bar{s}_1/\bar{s}_2$), α is the nodal point prefactor, and q_i is the water discharge per unit width in branch i. Equation (7) can also be written as

$$\bar{S}^* = \alpha Q^{*k} B^{*1-k}, \quad \text{or} \quad \frac{\bar{S}_1}{\bar{S}_2} = \alpha \left(\frac{Q_1}{Q_2}\right)^k \left(\frac{B_1}{B_2}\right)^{1-k} \tag{8}$$

For conditions dominated by two grain size modes (gravel and sand), we introduce two nodal point relations, one describing the partitioning of the gravel load over the bifurcates and one the sand load:

$$\bar{S}_g^* = \alpha_g Q^{*k_g} B^{*1-k_g}, \quad \text{or} \quad \frac{\bar{S}_{1g}}{\bar{S}_{2g}} = \alpha_g \left(\frac{Q_1}{Q_2}\right)^{k_g} \left(\frac{B_1}{B_2}\right)^{1-k_g} \tag{9}$$

$$\bar{S}_s^* = \alpha_s Q^{*k_s} B^{*1-k_s}, \quad \text{or} \quad \frac{\bar{S}_{1s}}{\bar{S}_{2s}} = \alpha_s \left(\frac{Q_1}{Q_2}\right)^{k_s} \left(\frac{B_1}{B_2}\right)^{1-k_s} \tag{10}$$

where k_g and k_s denote the nodal point coefficients and α_g and α_s are the nodal point prefactors, both for gravel and sand, respectively.

We realize that the above form of the nodal point relations is too simple to cover the physics of the problem of river bifurcations adequately. In addition to the strongly simplified form of the nodal point relations for gravel and sand, the values for the nodal point coefficients k_g, k_s, α_g, and α_s likely are not constants and models for these coefficients are needed to properly analyze the physics of the bifurcation problem. Yet despite these strong simplifications we believe that the current analysis provides useful insight on elementary bifurcation behavior. We will address this aspect in further detail in the discussion section.

The fact that both downstream branches are governed by the same base level (Figure 1) and also the upstream water surface elevation of the two branches is equal creates the following geometrical constraint in an equilibrium state (*Wang et al.*, 1995):

$$i^* = \frac{1}{L^*}, \quad \text{or} \quad \frac{i_1}{i_2} = \frac{L_2}{L_1} \tag{11}$$

where L_i is the length of branch i (Figure 1).

We now have a set of equations that can be solved to determine the equilibrium states of the two downstream branches.

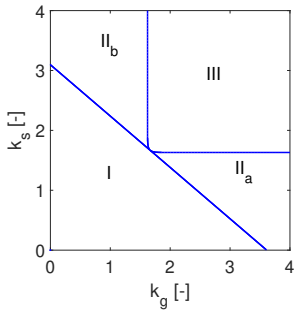

Figure 3: Sections I, II_a, II_b, and III in the stability diagram in the (k_g, k_s) parameter space for the base case.

3. The equilibrium state

We manipulate the set of equations listed in section 2 to find the equilibrium solutions of the bifurcation cases shown in Figure 1. Under equilibrium conditions the sediment supply rate must be equal to the sediment transport capacity and we therefore set $S_{ig} = \bar{S}_{ig}$ and $S_{is} = \bar{S}_{is}$. In addition, we substitute equations (2)-(6) and (11) into (9) and (10). This yields an implicit solution to the ratio of the water discharge in the two downstream branches, Q^*:

$$Q^* = L^* B^{*1-\frac{3}{n}} \left(\frac{m_g S_{s0} + m_s S_{g0}}{m_g S_{s0} \left(\alpha_s Q^{*k_s} B^{*1-k_s} + 1\right)^{-1} + m_s S_{g0} \left(\alpha_g Q^{*k_g} B^{*1-k_g} + 1\right)^{-1}} - 1 \right)^{\frac{3}{n}}$$
$$= \Phi(Q^*) \tag{12}$$

A solution of equation (12) provides values for the gravel and sand load in the downstream branches, S_{ig} and S_{is} $(i = 1, 2)$, through the nodal point relations in equations (9)-(10), provided that the water discharge in branch 0, Q_0, the gravel and sand supply rates to branch 0, S_{0g} and S_{0s}, and the variables m_g, m_s, L^*, B^*, k_s, and k_g are known. We compute the flow depth, H_i, using equation (3), as well as the surface gravel content, F_{ig}, using equation (5) or (6).

Equation (12) has at least three solutions: two solutions that are associated with the closure of one of the branches ($Q^* = 0$, $Q^* = \infty$) and one solution in which both downstream branches remain open. Generically the flow depth differs between the downstream branches, but under conditions in which $L^* = 1$ the flow depth in the downstream branches is equal, even if the width varies between the branches.

We define a base case that (except for the bifurcate length) is loosely based on the bifurcation of the Bovenrijn into the Pannerdensch Kanaal and the Waal branch. The bifurcation is located in the Netherlands and about 10 km downstream from where the Rhine River crosses the German-Dutch border. The water discharge is set equal to the one characterized by a one year recurrence period (4000 m^3/s). We simply assume the bifurcates to have the same channel length (here $L_1 = L_2 = 10$ km). This yields the following parameter values for

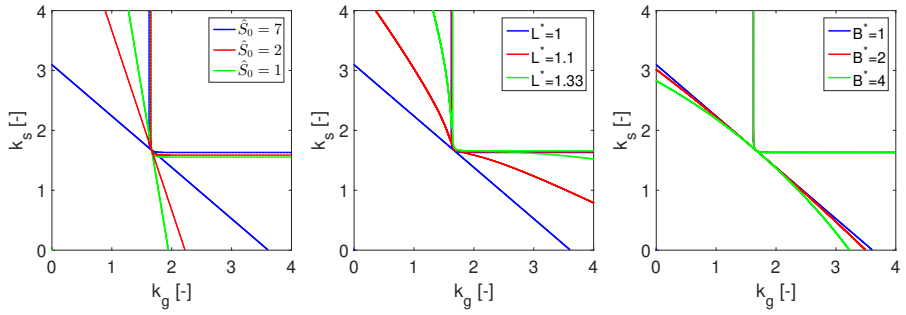

Figure 4: Stability diagram in the (k_g, k_s) parameter space, for varying (a) ratio of the sand load to the gravel load in branch 0, $\hat{S}_0$; (b) ratio of the length of the downstream channels, L^*; and (c) ratio of the width of the downstream channels, B^*.

the base case: $\alpha_g = \alpha_s = 1$, $B_0 = 315$ m, $B_1 = B_2 = 250$ m, $C_1 = C_2 = 50$ $\mathrm{m}^{1/2}/\mathrm{s}$, $S_{0g} = 0.001$ m^3/s, $S_{0s} = 0.007$ m^3/s, and $Q_0 = 4000$ m^3/s.

Analysis of equation (12) illustrates that we can distinguish between three sections in the (k_g, k_s) parameter space (I, II, and III), each with a different number of solutions to equation (12) and hence of the flow depth in the downstream branches (Figure 3):

- I and III: There are three equilibrium solutions. Two solutions correspond with one of the downstream branches closed. The other solution corresponds with both branches open.

- II_a and II_b: There are five equilibrium solutions. Two solutions correspond with one of the downstream branches closed. The remaining three solutions correspond with both branches open.

For the details of the analysis of equation (12) we refer to Appendix A.1. The differences between sections I and III and between II_a and II_b will be addressed in the next section.

The boundaries of the sections I, II_a, II_b, and III in Figure 3 depend on the ratio of the sand load to the gravel load in the upstream branch (branch 0), which is denoted by $\hat{S}_0$, the ratio of the length of the bifurcates, L^*, and the ratio of the channel width of the bifurcates, B^* (Figure 4). An increase of the sand load in the upstream channel at the expense of its gravel load leads to a decrease of section II_b and an increase of section II_a. An increase of the difference in channel length between the two bifurcates significantly decreases section II and an increase of section I. Section II tends to become negligible for values of L^* even mildly larger than 1. The effects of $\hat{S}_0$ and L^* are significant, whereas the effect of a difference in channel width between the two bifurcates, B^*, appears to be limited.

The current analysis is limited to engineered rivers where the channel width cannot adjust to changes in the controls (i.e., statistics of the water discharge,

sediment supply, and base level). The analysis illustrates that a mixed-size sediment two-channel system consists of three to five solutions to the morphodynamic equilibrium state. This differs from a unisize sediment two-channel system, for which three equilibrium solutions exist (*Wang et al.*, 1995). The existence of three to five solutions also contrasts with the single solution to the morphodynamic equilibrium state of a one-channel system, under unisize as well as mixed-size sediment conditions (*Howard*, 1980; *Blom et al.*, 2016, 2017a).

Natural rivers, where besides the channel slope and bed surface texture also the channel width responds to changes in the controls, allow for more equilibrium states than engineered rivers with a fixed channel width (*Blom et al.*, 2017a). In natural rivers there exists a range of equilibrium states for which the channel is able to transport the load supplied from above (*Blom et al.*, 2017a). In the current analysis we have not considered the effect of erodable banks, yet one may expect that, just as in the single channel case, the presence of erodable banks allows for a range of equilibrium states.

4. Model of the stability of the equilibrium state

We set up a system of differential equations for the flow depth and the surface gravel content in the bifurcates to study the temporal changes in the bifurcation system.

For simplicity, we assume that perturbations in bed elevation (i.e., aggradational and degradational waves), which arise from a difference between the sediment supply to a downstream branch and its sediment transport capacity, move so fast along the downstream branches that we can assume an instantaneous branch-averaged response of bed elevation. This implies that we consider branch-averaged values for bed elevation, η_i, flow depth, H_i, and surface texture represented by the surface gravel content, F_{ig} (Figure 2). Another consequence of this branch-averaged approach is the fact that the channel slope in each bifurcate cannot adjust with time, as the aggradation or degradation rate does not vary within a bifurcate. The constant channel slope and base level imply that, although the bed elevation changes with time, the water surface elevation in the bifurcates remains constant with time.

The Exner equation describing conservation of bed sediment is

$$c_b B_i \frac{\partial \eta_i}{\partial t} = -\frac{\partial S_i}{\partial x} \tag{13}$$

where t denotes time, c_b the sediment concentration within the bed ($c_b = 1 - p$ with p denoting bed porosity), and η is bed elevation with respect to a fixed reference level. As $H = \eta_w - \eta$ (Figure 2) and the water surface elevation, η_w, is constant due to our branch-averaged approach, we find that $\partial \eta_i / \partial t = -\partial H_i / \partial t$. This implies that equation (13) can be written as (*Wang et al.*, 1995):

$$c_b B_i \frac{\partial H_i}{\partial t} = \frac{\partial S_i}{\partial x} \tag{14}$$

As we assume that gradients in the sediment transport rate result in a branch-averaged degradation or aggradation rate, we write $\partial S_i/\partial x$ as

$$\frac{\partial S_i}{\partial x} = \frac{S_i - \bar{S}_i}{L_i} \tag{15}$$

Combination of equations (14) and (15) then yields

$$\frac{dH_i}{dt} = \frac{1}{c_b B_i L_i} \left(S_i - \bar{S}_i \right) \tag{16}$$

We apply a simplified form of the Hirano active layer model (*Hirano*, 1971) to describe the temporal change of the surface gravel content in the topmost part of the bed that interacts with the flow (i.e., in the active layer).

To arrive at a simplified version of the Hirano equation, we apply a similar branch-averaged approach to the migration of perturbations in the bed surface texture as to perturbations in bed elevation. Worded differently, we assume surface texture perturbations, which arise from a difference between the grain size distribution of the sediment supply to a downstream branch and the grain size distribution of the transported sediment, to move so fast along a bifurcate that we can consider a branch-averaged response of the bed surface gravel content in the bifurcate, F_{ig}.

In addition, we assume that the vertical sediment flux between the active layer and the substrate that is associated with a change in elevation of the interface between the active layer and the substrate has the same grain size distribution as the one of the active layer sediment, even under conditions of degradation.

Under these simplifying assumptions the Hirano active layer equation reduces to

$$\frac{dF_{ig}}{dt} = \frac{1}{c_b B_i L_i} \frac{1}{L_A} \left(F_{ig}(S_i - \bar{S}_i) + (\bar{S}_{ig} - S_{ig}) \right) \tag{17}$$

where L_A denotes the thickness of the active layer or the surface layer that is reworked by the flow.

This yields the following system of differential equations for the flow depth, H_i, and surface gravel content, F_{ig} by manipulating equations (16)-(17), using equations (9)-(10), for simplicity setting $\alpha_g = \alpha_s = 1$, and introducing time $\hat{t}$

where $\hat{t} = t/c_b$:

$$\frac{dH_1}{d\hat{t}} = \frac{Q_0^n}{B_1 L_1} \left(g_1(H_1, H_2, F_{1g}) - \bar{g}_1(H_1, H_2) \right) \tag{18}$$

$$\frac{dH_2}{d\hat{t}} = \frac{Q_0^n}{B_2 L_2} \left(g_2(H_1, H_2, F_{2g}) - \bar{g}_2(H_1, H_2) \right) \tag{19}$$

$$\frac{dF_{1g}}{d\hat{t}} = \frac{Q_0^n}{B_1 L_1} \frac{1}{L_A} (F_{1g} \left(g_1(H_1, H_2, F_{1g}) - \bar{g}_1(H_1, H_2) \right) + (\bar{g}_{1g}(H_1, H_2) - g_{1g}(H_1, H_2, F_{1g}))) \tag{20}$$

$$\frac{dF_{2g}}{d\hat{t}} = \frac{Q_0^n}{B_2 L_2} \frac{1}{L_A} (F_{2g} \left(g_2(H_1, H_2, F_{2g}) - \bar{g}_2(H_1, H_2) \right) + (\bar{g}_{2g}(H_1, H_2) - g_{2g}(H_1, H_2, F_{2g}))) \tag{21}$$

where the functions g_i, $\bar{g}_i$, g_{ig}, and $\bar{g}_{ig}$ $(i = 1, 2)$ are defined in Appendix B.

We abbreviate equations (18)-(21) by $(\dot{H}_i, \dot{F}_{ig}) = \Psi(H_i, F_{ig})$ where the dot indicates the derivative with respect to time. Naturally the equilibrium solutions of section 3 are solutions of $\Psi(H_i, F_{ig}) = 0$.

5. Stability of the equilibrium state

Equilibrium solutions only emerge if they are stable. The stability properties of the solutions of $\Psi(H_i, F_{ig}) = 0$ are determined by the eigenvalues of the Jacobian J of Ψ, which is defined as:

$$J = \begin{pmatrix} \frac{\partial \Psi_1}{\partial H_1} & \frac{\partial \Psi_1}{\partial H_2} & \frac{\partial \Psi_1}{\partial F_{1g}} & \frac{\partial \Psi_1}{\partial F_{2g}} \\ \frac{\partial \Psi_2}{\partial H_1} & \frac{\partial \Psi_2}{\partial H_2} & \frac{\partial \Psi_2}{\partial F_{1g}} & \frac{\partial \Psi_2}{\partial F_{2g}} \\ \frac{\partial \Psi_3}{\partial H_1} & \frac{\partial \Psi_3}{\partial H_2} & \frac{\partial \Psi_3}{\partial F_{1g}} & \frac{\partial \Psi_3}{\partial F_{2g}} \\ \frac{\partial \Psi_4}{\partial H_1} & \frac{\partial \Psi_4}{\partial H_2} & \frac{\partial \Psi_4}{\partial F_{1g}} & \frac{\partial \Psi_4}{\partial F_{2g}} \end{pmatrix} \tag{22}$$

If all eigenvalues at an equilibrium solution have negative (positive) real parts, the equilibrium solutions are linearly and nonlinearly stable (unstable), and are nodal points in the 4-dimensional phase space. If there are positive and negative eigenvalues, the solution is unstable and a saddle point in the phase space (e.g., *Wiggins*, 1990). Purely imaginaire eigenvalues would give rise to periodic solutions in the phase space, yet this does not occur for this particular set of equations.

As the system of equations (18)-(21) and the associated Jacobian J in equation (22) are too complex to be analyzed analytically, we analyze the system numerically. For the details of the analysis we refer to Appendix A.2. In summary, the following holds for the sections I-III in Figure 3:

- I: The two equilibrium solutions that correspond with one branch closed are stable. The other solution, where both branches are open, is unstable. The initial conditions determine to which stable state the system evolves.

- II_a and II_b: The two equilibrium solutions that correspond with one branch closed are stable. The other three solutions correspond with both branches open. The two 'new' solutions (compared to section I) are created in a blue sky bifurcation (Appendix A.2). Only one of them is stable. The initial conditions determine to which of the three stable equilibrium states the system evolves.

- III: The two equilibrium solutions that correspond with one branch closed are unstable. The solution with both branches open is the only stable solution. This implies that for every initial condition both branches remain open.

For a two-channel system under unisize sediment conditions, there exists one critical value of the nodal point coefficient k ($k = n/3$), below which the equilibrium solution with one closed bifurcation is stable (*Wang et al.*, 1995). For values of k larger than $n/3$ the equilibrium solution with two open bifurcates is stable. A case in which $k < n/3$ is similar to the current section I and the latter case is similar to the current section III. Under unisize sediment conditions section II does not exist.

For a single channel system with fixed banks the single solution to the equilibrium state is stable (*Howard*, 1980; *Blom et al.*, 2016, 2017a).

6. Evolution towards the stable equilibrium state

We numerically simulate the system of equations (18)-(21) to assess (1) the effects of the initial flow depth, H_1 and H_2, and the initial surface gravel content, F_{1g} and F_{2g}, in the bifurcating branches; (2) the mechanism that results in closure of one of the branches; and (3) the effects of the nodal point coefficients in combination with the sediment supply. We analyze these three aspects below.

Effect of the initial conditions in the bifurcating branches

In section II the initial conditions determine to which of the three stable equilibrium states the system evolves.

Figure 5 shows the results of two numerical runs of the system of equations (18)-(21), in which we assess the effects of the initial flow depth in the bifurcating branches, H_1 and H_2. The only difference between the two runs are the initial values of the flow depth, H_1 and H_2. It appears that a difference in the initial flow depth results in different behavior: in one case both branches stay open, while in the other case one branch closes.

In the case where both branches remain open, the surface gravel content in the two branches, F_{1g} and F_{2g}, evolves towards the same value. The surface gravel content F_{1g} in the closing branch evolves to 0, which means that eventually the bed surface in this closing branch consists of sand only.

Figure 6 shows the results of two runs where only the initial surface gravel content in the bifurcating channels, F_{1g} and F_{2g}, varies between the runs. Again

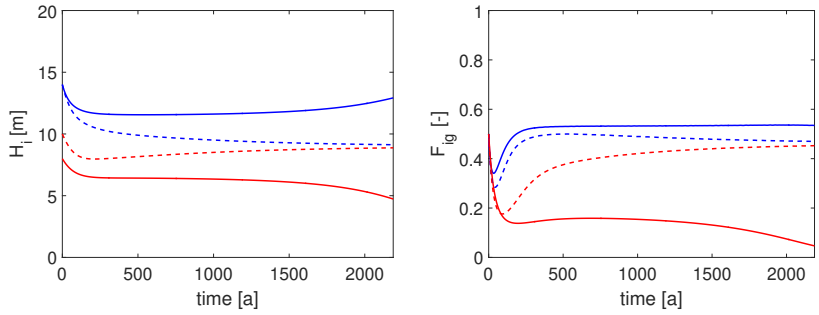

Figure 5: Effect of the initial flow depth in the downsteam channels on bifurcation dynamics. Flow depth H_1 and H_2 (left panel) and surface gravel content F_{1g} and F_{2g} (right panel) in the two downstream branches. Initially, $H_1 = 14$ m and $H_2 = 8$ m (solid lines) and $H_1 = 14$ m and $H_2 = 10$ m (dashed lines), and $F_{1g} = 0.5, F_{2g} = 0.5$. Blue and red lines indicate, respectively, branch 1 and branch 2. Results are given for $k_g = 3$, $k_s = 1$, $\alpha_g = \alpha_s = 1$, and $L_A = 1$ m. Here time indicates $\hat{t}$.

we observe the effect of the initial conditions: they determine whether the situation evolves towards a state with either both branches open or one branch closed.

Mechanism of closure of one of the branches

We consider the case where one of the branches closes in Figure 5 (solid lines) to study the mechanism of branch closure. To this end we analyze the difference between the load and supply of gravel and sand for, respectively, branches 1 and 2 (Figure 7a and b).

As the sediment supply in branch 2 exceeds the sediment transport capacity ($S_2 - \bar{S}_2 < 0$), aggradation will occur and branch 2 slowly closes. The sediment supply in branch 1 approaches the sediment transport capacity ($S_1 - \bar{S}_1 \downarrow 0$), which implies that the flow depth in branch 1 approaches an equilibrium (nonzero) value.

In branch 2 the sand supply exceeds the sand transport capacity ($S_{2s} - \bar{S}_{2s} < 0$) and the gravel supply is smaller than the gravel transport capacity ($S_{2g} - \bar{S}_{2g} > 0$), which implies that the bed surface of the branch becomes increasingly sandy. This is reflected by the fact that bed surface gravel content approaches zero ($F_{2g} \downarrow 0$, solid line in Figure 5b). The bed surface of branch 1 continues to consist of a mixture of gravel and sand (i.e., F_{1g} approaches an equilibrium nonzero value). This is understandable as in the final state the gravel and sand supply from the upstream branch is transported by branch 1, which requires both gravel and sand to be represented at the bed surface (see equations (5) and (6)).

Effects of nodal point coefficients and sediment supply

Finally we study the dependence of bifurcation dynamics on the nodal point coefficients, k_g and k_s, and the gravel and sand supply to the upstream branch

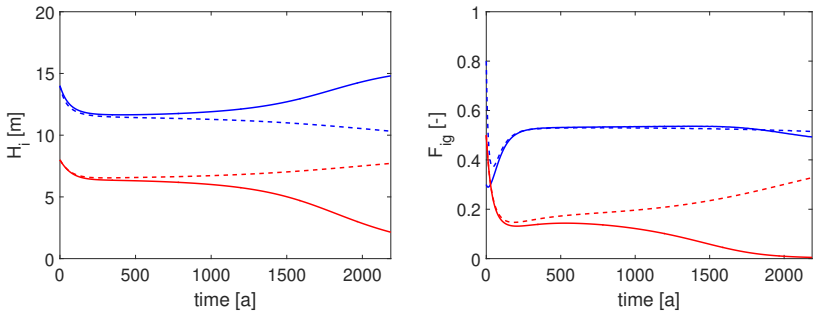

(a) (b)

Figure 6: Effect of the initial surface gravel content in the downsteam channels on bifurcation dynamics. Flow depth H_1 and H_2 (left panel) and surface gravel content F_{1g} and F_{2g} (right panel) in the two downstream branches. Initially, $F_{1g} = 0.8, F_{2g} = 0.5$ (dashed lines) and $F_{1g} = 0.3, F_{2g} = 0.5$ (solid lines), and $H_1 = 14$ m and $H_2 = 8$ m. Blue and red lines indicate, respectively, branch 1 and branch 2. Results are given for $k_g = 3$, $k_s = 1$, $\alpha_g = \alpha_s = 1$, and $L_A = 1$ m. Here time indicates $\hat{t}$.

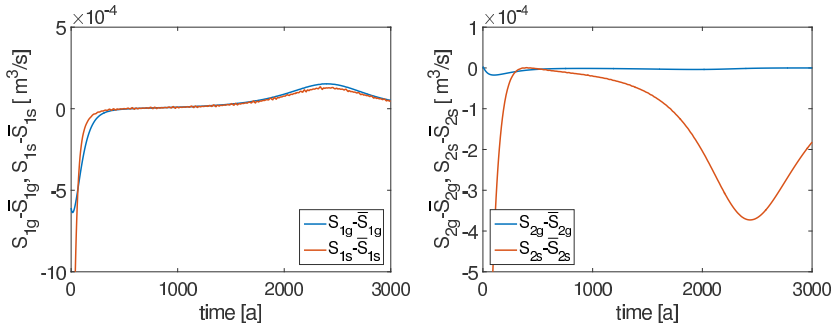

(a) (b)

Figure 7: Difference between the supply and transport capacity of gravel (blue line) and sand (red line) in branch 1 (left panel) and branch 2 (right panel). The conditions are equal to the case represented by the solid lines in Figure 5. Here time indicates $\hat{t}$.

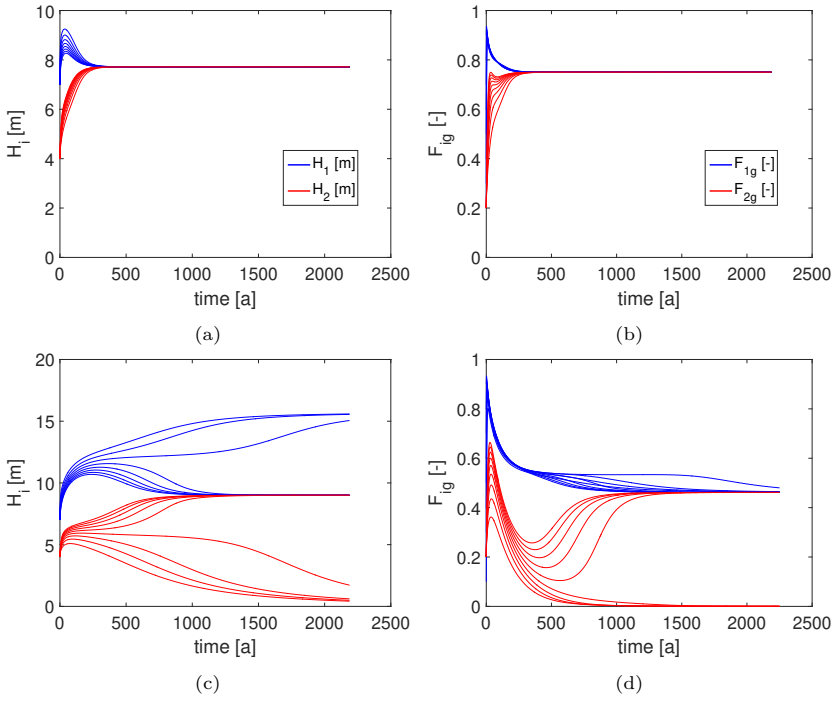

Figure 8: Effect of the gravel content in the sediment supply on bifurcation evolution for $k_g = 5, k_s = 1$ (section II$_a$): flow depth H_1 and H_2 (left panels) and surface gravel content F_{1g} and F_{2g} (right panels). Results are given for $\alpha_g = \alpha_s = 1$ and $L_A = 1$ m. Initially $0.1 \leq F_{1g} \leq 0.9$ and $F_{2g} = 0.2$. In upper panels $\hat{S}_0 = S_{0s}/S_{0g} = 2$ (i.e., a relatively coarse supply) and in lower panels $\hat{S}_0 = 7$ (i.e., a relatively fine supply). Blue and red lines indicate, respectively, branch 1 and branch 2. Here time indicates $\hat{t}$.

0. We consider two situations: $k_g = 5, k_s = 1$ (section II$_a$, Figure 8) and $k_g = 1, k_s = 5$ (section II$_b$, Figure 9). We study two cases with respect to the ratio $\hat{S}_0 = S_{0s}/S_{0g}$: either $\hat{S}_0 = 2$ (i.e., a relatively coarse supply, upper plots) or $\hat{S}_0 = 7$ (i.e., a relatively fine supply, lower plots).

If $k_g > k_s$ (Figure 8) a case governed by a relatively coarse sediment supply to the upstream branch tends towards a system with two stable open branches, and this change happens relatively fast. A case with a much larger sand content in the sediment supply tends to develop towards a system with one closed channel if the initial surface gravel content in branch 1 is in the range 0.1-0.4 (Figure 8c-d).

Yet, if $k_s > k_g$ (Figure 9), a case with a relatively coarse upstream supply tends towards a system with one closed channel provided that the initial gravel content in branch 1 is in the range 0.2-0.9 (Figure 9a-b). For a relatively fine sediment supply to the upstream branch, the situation with two open branches is always stable (Figure 9c-d).

Finally we stress the long time scale associated with the temporal change

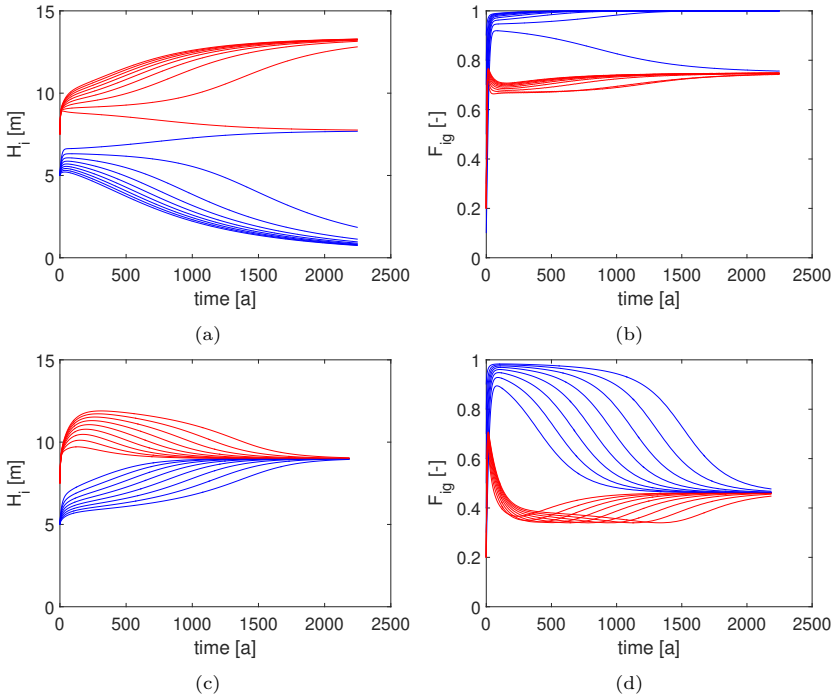

Figure 9: Effect of the gravel content in the sediment supply on bifurcation evolution for $k_g = 1, k_s = 5$ (section II_b): flow depth H_1 and H_2 (left panels) and surface gravel content F_{1g} and F_{2g} (right panels). Results are given for $\alpha_g = \alpha_s = 1$ and $L_A = 1$ m. Initially $0.1 \leq F_{1g} \leq 0.9$ and $F_{2g} = 0.2$. In upper panels $\hat{S}_0 = S_{0s}/S_{0g} = 2$ (i.e., a relatively coarse supply) and in lower panels $\hat{S}_0 = 7$ (i.e., a relatively fine supply). Blue and red lines indicate, respectively, branch 1 and branch 2. Here time indicates $\hat{t}$.

of the bifurcation system in our numerical runs. This seems to be due to our assumption of branch-averaged change in the two bifurcates, which slows down bifurcation adjustment. This is because in the branch-averaged model the result of a mismatch between the sediment supply to a bifurcate and its sediment transport capacity is distributed over the entire branch rather than the effect initially being limited to the upstream end of the bifurcate. In reality such a mismatch leads to an aggradational or degradational wave that starts at the upstream end of the bifurcate and then migrates downstream. This feeds back to the mismatch more strongly than in our branch-averaged approach and therefore in reality the expected change likely occurs much faster than in our idealized model. Nevertheless, there is evidence from field data that bifurcation change can be slow: a change to a new dominant channel may require significant time (*Slingerland and Smith*, 2004) and often require several centuries in the Rhine-Meuse delta, and durations of up to 1250 years have been estimated by *Stouthamer and Berendsen* (2001).

7. Discussion

The load relation

In our analysis we have applied the Engelund and Hansen load relation in a fractional manner (*Blom et al.*, 2016, 2017a). This fractional form of the load relation has never been properly validated and this approach likely is more valid in lowland rivers where partial mobility is less relevant. The analysis can be repeated for more complicated load relations (e.g., those including a threshold for significant transport or hiding effects). We do not expect, however, that application of a more complicated and realistic load relation affects our analysis and conclusions, as another load relation does not change the analysis in a fundamental manner. The analysis would still yield four coupled differential equations (similar to equations (18)-(21)), in which the coefficients are different from the ones based on the original load relation. This also holds for the Jacobian in equation (22). The results would differ somewhat from the ones based on the original load relation but we do not expect new phenomena.

The nodal point relation

A crucial point in the presented analysis is the fact that we assume that there exists a nodal point relation of the form of equation (8) for the unisize sediment case, or equations (9) and (10) for the mixed-size sediment case. This form of the nodal point relation is too simple to describe the partitioning of sediment at river bifurcations (e.g., *Van der Mark and Mosselman*, 2013). *Wang et al.* (1995) already suggested a nodal point relation of a more extensive form: $S^* = f(B^*, Q^*, C^*, H^*, ...)$. It is, however, difficult to constrain the various parameters in the nodal point relation, although an attempt may lead to a more realistic relation. Even in the simple form of the nodal point relation used here, the values of its coefficients k_g, k_s, α_g, and α_s are not likely constant and

models describing their temporal behavior are needed to properly analyze river bifurcation problems.

The simplicity of our nodal point relation, however, does enable us to assess a range of reasonable values for k in the unisize sediment case. Let us consider the general nodal point relation in equation (8) and assume that the bed-material load is primarily transported as bed load. If we consider a bifurcation point with a flat bed just upstream of the bifurcation point, the sediment supply to the downstream branches is likely distributed over the downstream branches according to their values of the channel width and so it may be argued that $\bar{S}^* = B^*$, and so $k = 0$ and $\alpha = 1$ (*Bolla Pittaluga et al.*, 2003). At the other side of the spectrum we consider a case where sediment is primarily transported as wash load and well distributed over the water column. In such a case the sediment supply to the downstream branches is likely partitioned over the downstream branches according to the ratio of the water discharge ($\bar{S}^* = Q^*$), which implies that $k = \alpha = 1$ (*De Heer and Mosselman*, 2004; *Dutta et al.*, 2017). Thus, we expect that the finer the sediment supply to branch 0, the larger is the value of k (within the range of 0 to 1). In reality, however, conditions are more complex due to the presence of a lateral bed slope, a bend, bars, or structures. We discuss the latter effects below, first for the unisize sediment case and subsequently for the mixed-size sediment case.

Typically the difference in bed elevation between the two bifurcates induces a lateral slope just upstream of the bifurcation. This slope effect increases the sediment supply to the deeper bifurcate and therefore acts as a stabilizing mechanism, as it counteracts further deepening of the deeper bifurcate. This effect needs to be accounted for when setting up a model for the nodal point coefficient.

Bends and bars affect the flow just upstream of the bifurcation and as such may affect the sediment partitioning over the downstream branches of the bifurcation. For instance, the sediment partitioning at a bifurcation that is located just downstream of a pointbar in an inner bend is affected by the associated secondary flow and the transverse gradient in bed elevation just upstream of the bifurcation.

The presence of a sill in the downstream branch 1 likely reduces the sediment supply to that branch (Figure 10a). Considering the nodal point relation in equation (7) and assuming that the sill's effect on the sediment supply is larger than on the water discharge, k must be larger than 1 and for a relatively high sill (with barely sediment supply to the specific channel) k should approach ∞.

A similar line of reasoning holds under mixed-size sediment conditions. Recall that the nodal point relations (equations (9) and (10)) read $\bar{s}_g^* = \alpha_g {q^*}^{k_g}$ and $\bar{s}_s = \alpha_s {q^*}^{k_s}$. The above lateral slope effect induced by the inlet step varies with grain size: coarse sediment is affected more strongly than fine sediment (*Parker and Andrews*, 1985), and the same holds for the lateral slope effect introduced by bends and bars. This also applies to the presence of a sill in one of the bifurcates: coarse sediment is affected more strongly than fine sediment, as the transport of coarse sediment concentrates more strongly near the bed. An

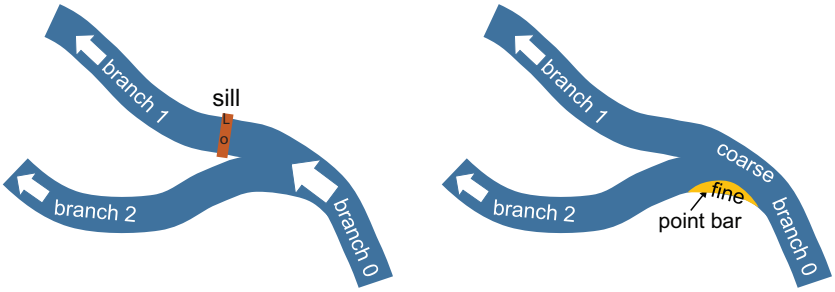

Figure 10: Schematic of two bifurcating branches with (a) a sill and (b) a point bar.

additional effect of a river bend is bend sorting. A pointbar typically consists of relatively fine sediment, whereas the bed surface and transported load in the outer bend are coarser (Figure 10b). Hence, the sediment supply to the bifurcate located in the outer bend is coarser than the supply to the other bifurcate. These effects will need to be accounted for in relations for the nodal point coefficients α_g, α_s, k_g, and k_s. The associated consequences for river bifurcation dynamics will need to be studied.

The stability criterion

Based on their mathematical stability analysis for the case of unisize sediment conditions, *Wang et al.* (1995) found that the stability criterion for two open branches is given by $k > n/3$. This can also be found through reasoning (*Kleinhans et al.*, 2008), which is summarized here to subsequently extend this reasoning to the case of mixed-size sediment. Equation (8) illustrates that the sediment supply to branch i, $\bar{s}_i$, is proportional to q_i^k, and equations (2)-(1) show that the sediment transport capacity of a branch is proportional to $q_i^{n/3}$. Now suppose that $k > n/3$. In that case the sediment supply per unit width to branch i increases more strongly with increasing water discharge per unit width in branch i, than the sediment transport capacity, which leads to aggradation. As a result the water discharge per unit width, q_i, decreases, which means that the situation stabilizes. On the other hand, if $k < n/3$, the sediment supply to branch i increases less strongly with increasing q_i than the sediment transport capacity. This implies that the channel degrades, which increases q_i even further. So the situation further destabilizes at the expense of the other downstream branch, which closes.

For the case of mixed-size sediment we reason in a similar manner. The supply of gravel and sand to branch i, $\bar{s}_{ig}$ and $\bar{s}_{is}$, are proportional to $q_i^{k_g}$ and $q_i^{k_s}$, respectively. The transport capacities of gravel and sand in branch i, s_{ig} and s_{is}, now also depend on the surface gravel content in branch i, F_{ig}, and are proportional to $F_{ig} m_g q_i^{n/3}$ and $(1 - F_{ig}) m_s q_i^{n/3}$, respectively. We now suppose that the water discharge per unit width in branch i, q_i, increases. This implies that the gravel and sand supply to branch i increase, the manner of which depend on the values of k_g and k_s. As k_g and k_s are expected to have different

values, the gravel and sand supply to branch i respond differently to the increase in the water discharge. Also the gravel and sand transport capacities, s_{ig} and s_{is}, respond differently to the increase in the water discharge due to the mobility difference between coarse and fine sediment (i.e., grain size selective transport). Depending on the resulting change of the gravel and sand supply to branch i, $\bar{s}_{ig}$ and $\bar{s}_{is}$, and the change in the gravel and sand transport capacities, s_{ig} and s_{is}, the increase in water discharge q_i affects the surface gravel content in branch i, F_{ig}, which is expressed by a coarsening or fining of the bed surface. Thus, based on physical reasoning it is much less straightforward to draw conclusions concerning the expected temporal change and a stability criterion of a river bifurcation dominated by mixed-size sediment.

As a next step we recommend the formulation of submodels for the nodal point coefficients k_g and k_s, which, among other parameters, likely depend on the transverse bed slope just upstream of the bifurcation (*Bolla Pittaluga et al.*, 2003) and hence likely are a function of the ratio of the flow depth in the bifurcates, H^* (where $H^* = H_1/H_2$). In such a case the formulation of the Jacobian in equation (22) becomes more complicated because of the derivatives with respect to H_1 and H_2. Analysis of the Jacobian and the numerical results would provide insight on the expected temporal change and the stability criterion of a river bifurcation dominated by mixed-size sediment.

Symmetrical bifurcations

It has been found that symmetrical bifurcations (i.e., bifurcates with equal properties such as water discharge, channel width, and flow depth) tend to be unstable more often than asymmetrical bifurcations (i.e., one of the bifurcates is significantly smaller than the other one) (*Miori et al.*, 2006; *Bertoldi and Tubino*, 2007; *Edmonds and Slingerland*, 2008; *Kleinhans et al.*, 2008, 2013; *Bolla Pittaluga et al.*, 2015). In our base case, which is characterized by equal channel width, friction, and length of the bifurcates, we find that in sections II and III symmetrical solutions are stable, which may contradict the above findings. Our results are similar to those of *Wang et al.* (1995), who find that a symmetrical solution is stable for $k > n/3$. This similarity between the results may not be surprising as our model is an extension of the highly idealized model of *Wang et al.* (1995) to mixed-size sediment conditions, whereas other models account for the effects of a transverse bed slope (*Bolla Pittaluga et al.*, 2003; *Edmonds and Slingerland*, 2008; *Kleinhans et al.*, 2008, 2013; *Bolla Pittaluga et al.*, 2015), alternate bars (*Bertoldi et al.*, 2009; *Redolfi et al.*, 2016), curvature-induced flow asymmetry upstream of the bifurcation (*Kleinhans et al.*, 2008; *Van Denderen et al.*, 2017), suspended bed-material load (*Slingerland and Smith*, 1998), cohesive sediment (*Edmonds and Slingerland*, 2008; *Hajek and Edmonds*, 2014), bend sorting (*Sloff et al.*, 2003; *Sloff and Mosselman*, 2012), and bank erosion (*Miori et al.*, 2006; *Van Denderen et al.*, 2017). These effects are not taken into account in our analysis but may be represented by appropriate future models for k_g and k_s.

8. Conclusions

We extend a highly idealized model of the dynamics of a river bifurcation to mixed-size sediment conditions. The model is based on nodal point relations for gravel and sand that set the partitioning of gravel and sand over the downstream branches or bifurcates. The model describes the equilibrium solutions and, based on a branch-averaged approximation of aggradation and degradation, describes the temporal change of bed elevation and bed surface texture in the bifurcates of a mixed-size sediment river bifurcation.

The introduction of mixed-size sediment mechanisms to the river bifurcation problem introduces an additional degree of freedom: the temporal adjustment of the bed surface texture in each of the bifurcates. The dynamics of the downstream branches concerning their flow depth and bed surface texture and the resulting stable configuration of the downstream branches result from differences between (a) the gravel and sand supply in each branch and (b) its gravel and sand transport capacity.

We set up a mathematical model of the equilibrium states and dynamics of a mixed-size sediment river bifurcation. In our analysis we have neglected the effects of a transverse bed slope, alternate bars, curvature-induced flow asymmetry upstream of the bifurcation, suspended bed-material load, cohesive sediment, bend sorting, and bank erosion. The proposed model therefore has limited predictive value regarding real river bifurcations, yet provides insight on the elementary effects of mixed-size sediment mechanisms on the river bifurcation problem. Subsequent analyses may combine the analysis of mixed-size sediment mechanisms with the above mentioned effects.

Howard (1980) and *Blom et al.* (2016, 2017a) have shown that there exists one solution to the morphodynamic equilibrium state in a one-channel system with nonerodible banks. In a unisize sediment two-channel system with fixed banks three equilibrium solutions exist, whereas three to five solutions exist in a mixed-size sediment bifurcation system.

In the mixed-size sediment two-channel system we distinguish three sections (I, II, and III) in the parameter space related to the nodal point coefficients. The specific layout of the three sections depends on the ratio of the bifurcate length and the ratio of the upstream gravel supply to the sand supply.

In section I the only stable solutions are the ones with one branch closed, and in section III the only stable solution is the one with both branches open. In section II there are three stable solutions: two with one branch closed and one with two open branches. To which of these three stable equilibrium solutions the system evolves depends on the initial conditions (i.e., the initial flow depth and bed surface texture in the bifurcates).

A. Details of the equilibrium solutions and their stability

A.1. Equilibrium solutions

In this appendix we analyze equation (12) and explain Figure 3 in more detail. The three solutions for Q^* of equation (12) give rise to three solutions

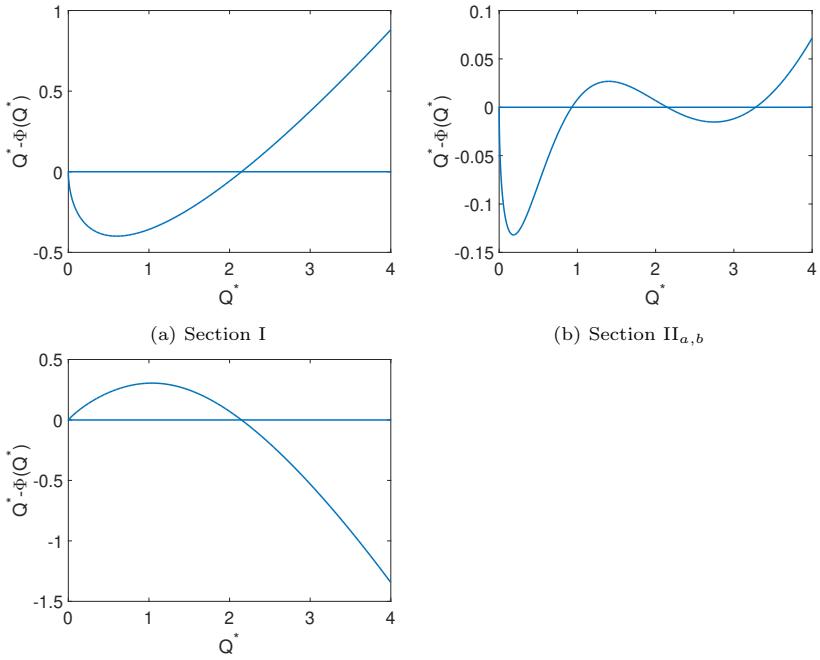

(a) Section I

(b) Section $\mathrm{II}_{a,b}$

(c) Section III

Figure 11: Typical graphs of $Q^* - \Phi(Q^*)$ for parameter values in sections I (left plot), $\mathrm{II}_{a,b}$ (centre plot) and III (right plot). Equilibrium solutions correspond with $Q^* - \Phi(Q^*) = 0$. $Q^* = 0$ and $Q^* = \infty$ are global solutions of $Q^* - \Phi(Q^*) = 0$.

for the combination of flow depths in the downstream branches H_i: two with one branch closed, one with both branches open. We now consider a fixed value of k_s and increase the value of k_g, i.e., we make a horizontal transect in Figure 3.

For relatively small values of k_s and k_g, three equilibrium solutions exist (Figure 11a). For such small values of k_s, there exists a threshold value for k_g ($k_g = k_{ga}$) for which there is a $\hat{Q}^*$ such that $\hat{Q}^* - \Phi(\hat{Q}^*) = 0$ and $d(Q^* - \Phi(Q^*))/dQ|_{Q^*=\hat{Q}^*} = 0$. This implies that for $k_g > k_{ga}$ two new solutions of $Q^* - \Phi(Q^*) = 0$ emerge and we then find five equilibrium solutions (Figure 11b): two with one branch closed and three with both branches open. The threshold value k_{ga} depends on k_s and defines the boundary between sections I and $\mathrm{II}_{a,b}$ in Figure 3.

For larger values of k_s, we find another threshold value for k_g, which we call k_{gb}. At that value, the new solutions of $Q^* - \Phi(Q^*) = 0$ that emerge at k_{ga} annilihate with $Q^* = 0$ and $Q^* = \infty$ (which correspond with one branch closed). So for larger values of k_s and for $k_g > k_{gb}$ there are again only 3 solutions (Figure 11c): two solutions correspond with the situation with a closed branch, and the other solutions with a situation with both branches open.

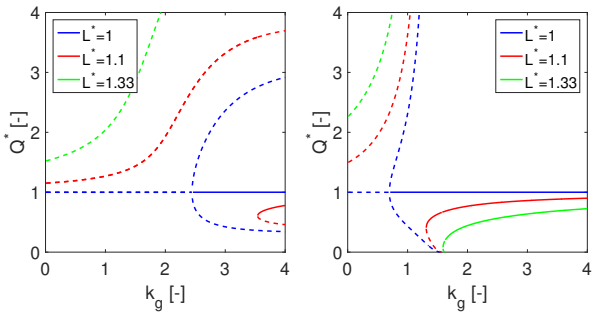

Figure 12: Bifurcation diagram for the equilibrium values of Q^* as a function of k_g for (a) $k_s = 1$ and (b) $k_s = 2.5$. Solid and dashed lines indicate, respectively, stable and unstable solutions. For simplicity the stable solutions $Q^* = 0$ and $Q^* = \infty$ are not shown.

A.2. Stability properties

This appendix explores the (k_s, k_g) parameter space and the stability properties of the equilibrium solutions in the sections I, II_a, II_b and III. We use the same approach as in appendix A: we fix k_s at a certain value and vary k_g (i.e., we again make a horizontal transect through Figure 3). For each combination of k_s and k_g, we determine where $Q^* - \Phi(Q^*) = 0$, compute the associated flow depth in the two bifurcates, H_i, and compute the other variables (e.g. S_{is}, S_{ig}, F_s, F_g etc) and the eigenvalues of the Jacobian J in equation (22).

Figure 12a shows the result for Q^* for $k_s = 1$ and $0 < k_g < 4$, for three values of L^*. For simplicity we do not indicate the stable solutions $Q^* = 0$ and $Q^* = \infty$. For each value of L^* one mathematical bifurcation occurs at a specific value of k_g (blue sky bifurcation, corresponding with the occurrence of the solid lines in Figure 12a). For $L^* = 1.33$ the bifurcation into a stable solution occurs for $k_g > 4$ in Figure 12a and is therefore not visible. The values of k_g for which the bifurcations occur correspond with the transitions from section I to II_a in Figure 3.

Figure 12b shows a similar plot for $k_s = 2.5$. Now we observe two bifurcations: one where the stable solution for Q^* emerges in a blue sky bifurcation (occurrence of the solid lines in Figure 12b), and one where the unstable solutions of Q^* are annihilated in a collision with the stable solutions $Q^* = 0$ and $Q^* = \infty$ (saddle-node bifurcation, vanishing of the dashes lines at $Q^* = 0$), leaving only one single stable solution in section III. We summarize the consequences of these results in section 5.

B. Functions in the system of equations

This appendix provides the functions for g_1, g_{1g}, g_2, g_{2g}, $\bar{g}_1$, $\bar{g}_{1g}$, $\bar{g}_2$, and $\bar{g}_{2g}$, required in the system described by equations (18)-(21):

$$g_1(H_1, H_2, F_{1g}) = (m_g F_{1g} + m_s(1 - F_{1g})) \frac{\gamma_1 H_1^{(n/2)}}{\left(\beta_1 H_1^{(3/2)} + \beta_2 H_2^{(3/2)}\right)^n}$$

$$g_{1g}(H_1, H_2, F_{1g}) = m_g F_{1g} \frac{\gamma_1 H_1^{(n/2)}}{\left(\beta_1 H_1^{(3/2)} + \beta_2 H_2^{(3/2)}\right)^n}$$

$$g_2(H_1, H_2, F_{2g}) = (m_g F_{2g} + m_s(1 - F_{2g})) \frac{\gamma_2 H_2(n/2)}{\left(\beta_1 H_1^{(3/2)} + \beta_2 H_2^{(3/2)}\right)^n}$$

$$g_{2g}(H_1, H_2, F_{2g}) = m_g F_{2g} \frac{\gamma_2 H_2(n/2)}{\left(\beta_1 H_1^{(3/2)} + \beta_2 H_2^{(3/2)}\right)^n}$$

$$\bar{g}_1(H_1, H_2) = \frac{B_0^{(1-n)}}{H_0^n} \left(\frac{f_g(H_1, H_2) F_{0g} m_g}{1 + f_g(H_1, H_2)} + \frac{f_s(H_1, H_2)(1 - F_{0g}) m_s}{1 + f_s(H_1, H_2)} \right)$$

$$\bar{g}_{1g}(H_1, H_2) = \frac{B_0^{(1-n)}}{H_0^n} \left(\frac{f_g(H_1, H_2) F_{0g} m_g}{1 + f_g(H_1, H_2)} \right)$$

$$\bar{g}_2(H_1, H_2) = \frac{B_0^{(1-n)}}{H_0^n} \left(\frac{F_{0g} m_g}{1 + f_g(H_1, H_2)} + \frac{(1 - F_{0g}) m_s}{1 + f_s(H_1, H_2)} \right)$$

$$\bar{g}_{2g}(H_1, H_2) = \frac{B_0^{(1-n)}}{H_0^n} \left(\frac{F_{0g} m_g}{1 + f_g(H_1, H_2)} \right)$$

where

$$\beta_i = B_i C L_i^{(-1/2)}, \quad i = 1, 2$$

$$\gamma_i = B_i C^n L_i^{(-n/2)}, \quad i = 1, 2$$

and

$$f_g(H_1, H_2) = \bar{S}_g^* = \frac{\bar{S}_{1g}}{\bar{S}_{2g}} = H^{*3k_g/2} B^{*1-k_g} \left(\frac{B^*}{\sqrt{L^*}} \right)^{k_g}$$

$$f_s(H_1, H_2) = \bar{S}_s^* = \frac{\bar{S}_{1s}}{\bar{S}_{2s}} = H^{*3k_s/2} B^{*1-k_s} \left(\frac{B^*}{\sqrt{L^*}} \right)^{k_s}$$

which follows from substitution of equations (2)-(3) and (11) into equations (9)-(10).

References

Bertoldi, W., and M. Tubino (2005), Bed and bank evolution of bifurcating channels, *Water Resour. Res.*, *41*(7), W07001, doi:10.1029/2004WR003333.

Bertoldi, W., and M. Tubino (2007), River bifurcations: Experimental observations on equilibrium configurations, *Water Resour. Res.*, *43*, doi:10.1029/2007WR005907.

Bertoldi, W., L. Zanoni, S. Miori, R. Repetto, and M. Tubino (2009), Interaction between migrating bars and bifurcations in gravel bed rivers, *Water Resour. Res.*, *45*(6), W06418, doi:10.1029/2008WR007086.

Blom, A., E. Viparelli, and V. Chavarrías (2016), The graded alluvial river: Profile concavity and downstream fining, *Geophys. Res. Lett.*, *43*, doi:10.1002/2016GL068898.

Blom, A., L. Arkesteijn, V. Chavarrías, and E. Viparelli (2017a), The equilibrium alluvial river under variable flow and its channel-forming discharge, *J. Geophys. Res., Earth Surface*, *122*, doi:10.1002/2017JF004213.

Blom, A., V. Chavarrías, R. I. Ferguson, and E. Viparelli (2017b), Advance, retreat, and halt of abrupt gravel-sand transitions in alluvial rivers, *Geophys. Res. Lett.*, *44*, doi:10.1002/2017GL074231.

Bolla Pittaluga, M., R. Repetto, and M. Tubino (2003), Channel bifurcation in braided rivers: Equilibrium configurations and stability, *Water Resour. Res.*, *39*(3), 1046, doi:10.1029/2001WR001112.

Bolla Pittaluga, M., G. Coco, and M. G. Kleinhans (2015), A unified framework for stability of channel bifurcations in gravel and sand fluvial systems, *Geophys. Res. Lett.*, *42*(18), 7521–7536, doi:10.1002/2015GL065175.

Bulle, H. (1926), Untersuchungen über die Geschiebeableitung bei der Spaltung von Wasserläufen: Modellversuche aus dem Flussbaulaboratorium der Technischen Hochschule zu Karlsruhe, *VDI Verlag, Berlin*, (in German).

Burge, L. M. (2006), Stability, morphology and surface grain size patterns of channel bifurcation in gravel-cobble bedded anabranching rivers, *Earth Surf. Process. Landf.*, *31*(10), 1211–1226, doi:10.1002/esp.1325.

Church, M. (2006), Bed material transport and the morphology of alluvial river channels, *Annu. Rev. Earth Planet. Sci.*, *34*, doi:10.1146/annurev.earth.33.092203.122721.

De Heer, A., and E. Mosselman (2004), Flow structure and bedload distribution at alluvial diversions, in *River Flow 2004, Proc. 2nd Int. Conf. Fluvial Hydraulics*, Napoli, Italy.

Dutta, S., D. Wang, P. Tassi, and M. H. Garcia (2017), Three-dimensional numerical modeling of the bulle effect: the nonlinear distribution of near-bed sediment at fluvial diversions, *Earth Surf. Process. Landf.*, doi:10.1002/esp.4186.

Edmonds, D. A., and R. L. Slingerland (2008), Stability of delta distributary networks and their bifurcations, *Water Resour. Res.*, *44*(9), W09426, doi:10.1029/2008WR006992.

Engelund, F., and E. Hansen (1967), Monograph on sediment transport in alluvial streams, *Tech. Rep.*, Hydraul. Lab., Tech. Univ. of Denmark, Copenhagen, Denmark, 63 pp.

Federici, B., and C. Paola (2003), Dynamics of channel bifurcations in noncohesive sediments, *Water Resour. Res.*, *39*(6), 1162, doi:10.1029/2002WR001434.

Frings, R., and M. Kleinhans (2008), Complex variations in sediment transport at three large river bifurcations during discharge waves in the river rhine, *Sedimentology*, *55*(5), 1145–1171, doi:10.1111/j.1365-3091.2007.00940.x.

Hackney, C. R., S. E. Darby, D. R. Parsons, J. Leyland, R. Aalto, A. P. Nicholas, and J. L. Best (2017), The influence of flow discharge variations on the morphodynamics of a diffluence-confluence unit on a large river, *Earth Surf. Process. Landf.*, doi:10.1002/esp.4204.

Hajek, E., and D. Edmonds (2014), Is river avulsion style controlled by floodplain morphodynamics?, *Geology*, *42*(3), 199–202, doi:10.1130/G35045.1.

Hardy, R. J., S. N. Lane, and D. Yu (2011), Flow structures at an idealized bifurcation: a numerical experiment, *Earth Surf. Process. Landf.*, *36*(15), 2083–2096, doi:10.1002/esp.2235.

Hirano, M. (1971), River bed degradation with armoring, *Trans. Jpn. Soc. Civ. Eng*, *3*(2), 194–195.

Howard, A. D. (1980), Thresholds in river regimes, in *Thresholds in Geomorphology*, Coates, D. R. and J. D. Vitek (eds.), pp. 227–258, Allen and Unwin, Boston.

Kleinhans, M. G., H. R. A. Jagers, E. Mosselman, and C. J. Sloff (2008), Bifurcation dynamics and avulsion duration in meandering rivers by one-dimensional and three-dimensional models, *Water Resour. Res.*, *44*, W08454, doi:10.1029/2007WR005912.

Kleinhans, M. G., R. I. Ferguson, S. N. Lane, and R. J. Hardy (2013), Splitting rivers at their seams: bifurcations and avulsion, *Earth Surf. Process. Landf.*, *38*(1), 47–61, doi:10.1002/esp.3268.

Lanzoni, S. (2000), Experiments on bar formation in a straight flume: 2. Graded sediment, *Water Resour. Res.*, *36*(11), 3351–3363, doi:10.1029/2000WR900161.

Marra, W. A., D. R. Parsons, M. G. Kleinhans, G. M. Keevil, and R. E. Thomas (2014), Near-bed and surface flow division patterns in experimental river bifurcations, *Water Resour. Res.*, *50*(2), 1506–1530, doi:10.1002/2013WR014215.

Miori, S., R. Repetto, and M. Tubino (2006), A one-dimensional model of bifurcations in gravel bed channels with erodible banks, *Water Resour. Res.*, *42*, W11413, doi:10.1029/2006WR004863.

Mosselman, E., and K. Sloff (2008), The importance of floods for bed topography and bed sediment composition: Numerical modelling of Rhine bifurcation at Pannerden, in *Gravel-Bed Rivers VI: From Process Understanding to River Restoration*, Elsevier, 161–179, doi:10.1016/S0928-2025(07)11124-X.

Paola, C. (2001), Modelling stream braiding over a range of scales, in *Gravel-bed Rivers V*, Mosley, M.P. (ed.), pp. 11–46, Wellington, New Zealand Hydrological Society.

Parker, G. (1991), Selective sorting and abrasion of river gravel. I: Theory, *J. Hydraul. Eng.*, *117*(2), 131–147, doi:10.1061/(ASCE)0733-9429(1991)117:2(131).

Parker, G., and E. D. Andrews (1985), Sorting of bed load sediment by flow in meander bends, *Water Resour. Res.*, *21*(9), 1361–1373, doi:10.1029/WR021i009p01361.

Ramamurthy, A. S., J. Qu, and D. Vo (2007), Numerical and experimental study of dividing open-channel flows, *J. Hydraul. Eng.*, *133*(10), 1135–1144, doi:10.1061/(ASCE)0733-9429(2007)133:10(1135).

Redolfi, M., G. Zolezzi, and M. Tubino (2016), Free instability of channel bifurcations and morphodynamic influence, *J. Fluid. Mech.*, *799*, 476–504, doi:10.1017/jfm.2016.389.

Ribberink, J. S. (1987), Mathematical modelling of one-dimensional morphological changes in rivers with non-uniform sediment, Ph.D. thesis, 206 pp., Delft University of Technology, The Netherlands.

Saint-Venant, A. J. C. B. (1871), Théorie du mouvement non permanent des eaux, avec application aux crues des rivières et à l'introduction des marées dans leur lit, *Comptes Rendus des séances de l'Académie des Sciences*, *73*, 237–240 (in French).

Sinha, S. K., and G. Parker (1996), Causes of concavity in longitudinal profiles of rivers, *Water Resour. Res.*, *32*(5), 1417–1428, doi:10.1029/95WR03819.

Slingerland, R., and N. D. Smith (1998), Necessary conditions for a meandering-river avulsion, *Geology*, *26*(5), 435–438, doi:10.1130/0091-7613(1998)026⟨0435:NCFAMR⟩2.3.CO;2.

Slingerland, R., and N. D. Smith (2004), River avulsions and their deposits, *Annu. Rev. Earth Planet. Sci.*, *32*(1), 257–285, doi:10.1146/annurev.earth.32.101802.120201.

Sloff, K., and E. Mosselman (2012), Bifurcation modelling in a meandering gravel-sand bed river, *Earth Surf. Process. Landf.*, *37*(14), 1556–1566, doi: 10.1002/esp.3305.

Sloff, K., M. Bernabè, and T. Baur (2003), On the stability of the Pannerdense Kop river bifurcation, in *Proc. 3rd IAHR Symposium on River, Coastal, and Estuarine Morphodynamics (RCEM), Barcelona*.

Stouthamer, E., and H. J. Berendsen (2001), Avulsion frequency, avulsion duration, and interavulsion period of Holocene channel belts in the Rhine-Meuse delta, The Netherlands, *J. Sediment. Res.*, *71*(4), 589–598, doi: 10.1306/112100710589.

Tarekul Islam, G. M., M. R. Kabir, and A. Nishat (2006), Nodal point relation for the distribution of sediments at channel bifurcation, *J. Hydraul. Eng.*, *132*(10), 1105–1109, doi:10.1061/(ASCE)0733-9429(2006)132:10(1105).

Thomas, R. E., D. R. Parsons, S. D. Sandbach, G. M. Keevil, W. A. Marra, R. J. Hardy, J. L. Best, S. N. Lane, and J. A. Ross (2011), An experimental study of discharge partitioning and flow structure at symmetrical bifurcations, *Earth Surf. Process. Landf.*, *36*(15), 2069–2082, doi:10.1002/esp.2231.

Tubino, M., and W. Bertoldi (2008), Bifurcations in gravel-bed streams, in *Gravel-Bed Rivers VI: From Process Understanding to River Restoration*, Elsevier, 133–159, doi:10.1016/S0928-2025(07)11123-8.

Van Denderen, R. P., R. M. J. Schielen, A. Blom, S. J. M. H. Hulscher, and M. G. Kleinhans (2017), Morphodynamic assessment of side channel systems using a simple one-dimensional bifurcation model and a comparison with aerial images, *Earth Surf. Process. Landf.*, doi:10.1002/esp.4267.

Van der Mark, C. F., and E. Mosselman (2013), Effects of helical flow in one-dimensional modelling of sediment distribution at river bifurcations, *38*, 502–511, doi:10.1002/esp.3335.

Van Dijk, W. M., F. Schuurman, W. I. van de Lageweg, and M. G. Kleinhans (2014), Bifurcation instability and chute cutoff development in meandering gravel-bed rivers, *Geomorphology*, *213*, 277–291, doi:10.1016/j.geomorph.2014.01.018.

Wang, Z., M. D. Vries, R. Fokkink, and A. Langerak (1995), Stability of river bifurcations in 1D morphodynamic models, *J. Hydraul. Res.*, *33*(6), 739–750, doi:10.1080/00221689509498549.

Wiggins, S. (1990), Introduction to Applied Nonlinear Dynamical Systems and Chaos, Springer-Verlag, New York.

Zolezzi, G., W. Bertoldi, and M. Tubino (2006), Morphological analysis and prediction of river bifurcations, in *Braided Rivers: Process, Deposits, Ecology and Management*, Wiley-Blackwell, IAS Special Publ., *36*, 233–256.